Optical Engineering

OpticalEngineering.SPIEDigitalLibrary.org

# Robust defect detection in plain and twill fabric using directional Bollinger bands

Henry Y. T. Ngan
Grantham K. H. Pang

SPIE.

# Robust defect detection in plain and twill fabric using directional Bollinger bands

**Henry Y. T. Ngan**[a,*] **and Grantham K. H. Pang**[b]
[a]Hong Kong Baptist University, Department of Mathematics, Kowloon Tong, Hong Kong
[b]University of Hong Kong, Department of Electrical and Electronic Engineering, Industrial Automation Research Laboratory, Pokfulam Road, Hong Kong

**Abstract.** A directional Bollinger bands (BB) method for the detection of defects in plain and twill fabric is presented, whereas a previous BB method was for patterned Jacquard fabric. BB are constructed using the moving average and standard deviation to characterize any irregularities (i.e., defects) in a patterned texture. Every patterned texture constitutes a primitive unit that can be used to generate the texture by a translational rule. The regularity property for a patterned texture can be implicitly regarded as the periodic signals on the rows and columns of an image. To utilize such a regularity property, an embedded shift-invariant characteristic of BB is explored. The original BB method is further developed using directional rotation iterations, which enables the detection of directional defects in plain and twill fabric. The directional BB method is an efficient, fast, and shift-invariant approach that enables defective regions to be clearly outlined. This approach is also immune to the alignment problem that often arises in the original method. The detection accuracies for 77 defective images and 100 defect-free images are 96.1% and 96%, respectively. In a pixel-to-pixel evaluation comparing the detection results of the defective images with the ground-truth images, a 93.51% detection success rate is achieved.
 [DOI: 10.1117/1.OE.54.7.073106]

Keywords: Bollinger bands; regularity property; shift-invariant property; rotational property; fabric inspection; texture analysis.

Paper 141921 received Dec. 16, 2014; accepted for publication Jun. 10, 2015; published online Jul. 13, 2015.

## 1 Introduction

Automated fabric inspection using automatic visual inspection (AVI) has been a popular research topic in the fields of automation and image processing for several decades. AVI can be facilitated using either an on-loom or off-loom inspection machine equipped with overhead digital cameras to monitor the manufacturing product. The automated inspection process aims to reduce manufacturing defects, improve product quality, reduce labor costs and time, and decrease the level of human inspection error. The traditional human inspection approach is controversial as it depends on the experience of skilled workers and only results in about 60% to 75% of defects[1] being eliminated. The AVI methods for fabric can be broadly classified into two main groups, motif-based[2] and nonmotif-based, based on the fundamental structure of a patterned texture, which is termed the motif. All patterned textures can be classified into 17 wallpaper groups[2] based on a motif which can be either a rectangular, square, or triangular shape. Each motif can generate a patterned texture for one particular wallpaper group by predefined symmetry rules: translation, rotation, reflection, and glide-reflection. Figure 1 illustrates the defective samples of plain and twill fabric (or so-called unpatterned fabric) that are examined in this paper. Under the wallpaper group classification, the plain and twill fabric belong to the p1 group, which is the most popular research target. Most of the developed detection methods can be classified into five main groups, the statistical, spectral, model-based, learning, and structural approaches. Some of the existing methods are capable of producing outstanding results; for example, the wavelet-based method[3] and the neural network (NN) method,[4] were shown to have accuracies of 95.8% and 94.38%, respectively. The previous Bollinger bands (BB) method[5] was designed for other patterned fabrics in the p2, pmm, and p4m groups and has obtained satisfactory detection results. In this paper, we extend the existing BB method for patterned fabrics to defect detection in plain and twill fabric.

Although the BB approach was originally developed for financial technical analysis, it has proven to be very effective and efficient in analyzing patterned fabrics. Mathematically, the BB approach is essentially composed of the moving average and standard deviation. The BB method extracts the upper and lower BB and applies these two bands to every detected image. By fast training with several defect-free samples, the maximum and minimum values of the upper and lower bands are learned as the threshold set. The BB method has embedded shift-invariant properties and can effectively characterize periodic patterned textures. The BB method has been shown to perform robustly for dot-, star-, and box-patterned fabrics. However, it remains unknown whether BB can also be applied to twill and plain fabric. In a preliminary evaluation, the BB method failed to recognize some defective samples. For example, as Fig. 2 shows, the BB method is weak at differentiating defects with directional features, such as the diagonal strips on the incorrect draw in Fig. 2(a). The discriminatory power of the BB method is sharpened when a defect appears orthogonally to the movement (i.e., horizontal or vertical direction) of the BB calculation. Figure 6 in Sec. 3 will demonstrate such an effect. Therefore, research is needed to optimize the discriminative power of the BB approach.

*Address all correspondence to: Henry Y. T. Ngan, E-mail: ytngan@hkbu.edu.hk

0091-3286 /2015/$25.00 © 2015 SPIE

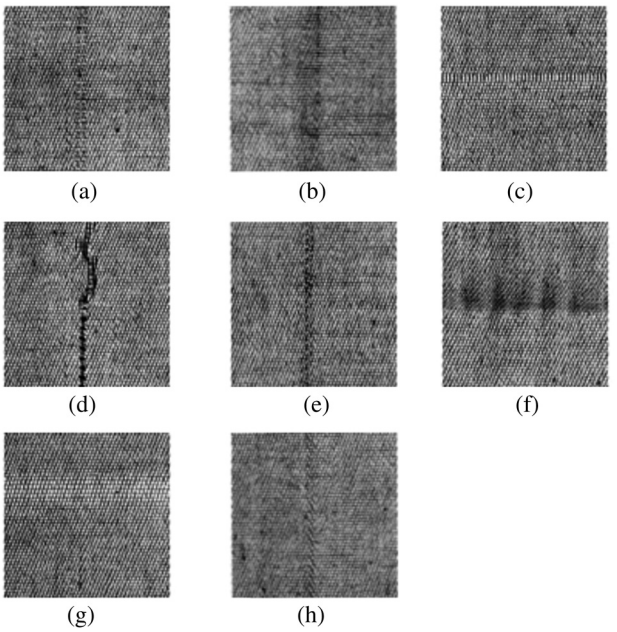


**Fig. 1** Samples of plain and twill fabric: (a) broken end (bn1), (b) dirty yarn (dy1), (c) mispick (mp1), (d) netting multiple (n1), (e) slack end (se1), (f) thick bar B (tkbb1), (g) thin bar (tn1), and (h) incorrect draw (wd1).

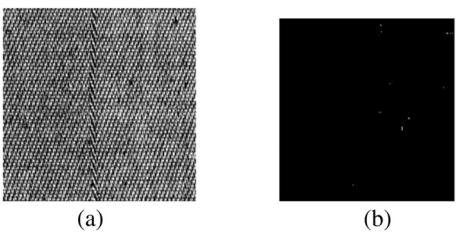


**Fig. 2** Failure of the Bollinger bands (BB) approach in detecting a defective image in the original orientation: (a) sample of wrong draw (wd6) and (b) detection result after the BB method.

The directional BB approach presented in this paper further extends the regularity property of the existing BB method to directional defects. First, every input image is rotated along four orientations: $\theta = 0$, 30, 45, and 60 deg. Every rotated image is then cropped to a standard size and processed by the upper and lower bands of the BB on the rows and columns, respectively. Next, the processed upper and lower bands undergo thresholding using the set of threshold values obtained from the training stage. Four intermediate binary images are generated, for which 1 (white pixels) denotes a defective pixel and 0 (dark pixel) denotes a defect-free pixel. One of the four intermediate images is selected as the final image by comparing the maximum number of white pixels.

This paper makes the following contributions to the literature:

1. The directional BB method, developed with four rotational representations, is shown to be a shift-invariant and fast fabric defect detection approach that is effective on the most popular plain and twill fabric.
2. A sound theoretical foundation of the BB method is constructed, which describes the regularity property of patterned textures, the invariant property of the BB method on patterned textures, the formulation of the defect detection rules, and the directional rotational approach, and provides strong theoretical support for the previous results.[5]
3. The detection accuracies for the plain and twill fabric reach 96.1% for defective images and 96% for defect-free images. The original BB method is based on the classical statistical measures of the moving average and standard deviation. However, it is weak at dealing with directional defects. The directional BB method presented in this paper can deal with less-prominent directional defects and, hence, is a significant advance on the existing models.
4. The directional BB method successfully extends the original BB approach and is evaluated using a ground-truth database of eight types of defective images, which is rare in the literature on unpatterned fabric inspection. In a pixel-to-pixel ground-truth evaluation, an average of 93.51% is obtained, which demonstrates the robustness of the directional BB method.

The remainder of this paper is organized as follows. In Sec. 2, we survey the literature on defect detection in plain and twill fabric. Section 3 outlines the directional BB method and its procedure. In Sec. 4, we evaluate the performance of the directional BB method for plain and twill fabric. Finally, Sec. 5 concludes the paper.

## 2 Literature Review on Defect Detection in Plain and Twill Fabric

As this paper is concerned with detecting defects in plain and twill fabric (the p1 group), the literature review focuses on the existing methodologies for defect detection in this fabric group. For fabric defect detection in the other 16 wallpaper groups, a number of methods have recently been developed, such as the wavelet-preprocessed golden image subtraction method,[6] the regular bands method,[7] the co-occurrence matrix method,[8] the local binary patterns method,[9] and the motif-based method.[2,10] Although plain and twill fabric are the most commonly used fabric in fabric defect detection, only a few methods have demonstrated good results.

The Fourier transform (FT) is a spectral approach that is commonly used for defect detection in plain and twill fabric.[11–16] The spatial domain is generally sensitive to noise and small amount of noises could affect the color distribution and deteriorate an image quality, making it challenging to identify defects. However, the FT characterizes defects in the frequency domain because defect-free patterns always demonstrate a similar spectrum regardless of the presence or absence of noise. A central spatial frequency spectrum[16] was proposed for plain fabric defect classification with seven parameters for outstanding characteristics. However, only a few defective samples from four classes of plain fabric defect were tested. The Gabor transform is another popular spectral approach for fabric inspection. Three detection schemes[17] using Gabor wavelet features have been proposed for plain and twill fabric. In the first, a supervised defect segmentation was performed using a threshold value based on the magnitude of the Gabor filtered images of defect-free samples. The

second involved an unsupervised web defect segmentation with a multichannel filtering approach that permitted a multiresolution analysis resembling the approach of Jain and Farrokhnia.[18] The test method used defective images from four twill and four plain weave fabrics. Both of these schemes enabled the defects to be outlined after segmentation. In the third approach, a fast web inspection was conducted using only the imaginary Gabor function with two one-dimensional projection signals on the rows and columns. This scheme was able to detect and locate most defects in the horizontal and vertical directions in 13 images (of various defects), although the explicit shapes were not shown. As Gabor transform indeed is a special case of short-time FT, it inherits it advantages and disadvantages. However, the reliability of the three schemes has yet to be addressed. In addition, there are other Gabor-based fabric inspection methods.[19–22]

Wavelets are often used in the feature extraction for plain and twill fabric inspection. Wavelet transforms (WTs) could remove noises on the background texture in their approximated subimages and extract the texture details by using horizontal, vertical, or/and diagonal detailed subimages. Hence, the onboard fabric defect detection machine using WT and edge fusion as preprocessing tools[23,24] was able to suppress the background texture and enhance the defect appearance on spun-yarn, filament-yarn, and sheeting fabrics. The defect detection, which was achieved by determining any nonhomogeneous regions after thresholding, provided 89% accuracy from a database of 26 defect types. A fine resolution vibration-free 4096-element line-scan camera was installed to identify any defects in the weave. Despite the fair accuracy rate, this method is one of the few to have been evaluated with a large test sample.

In general, the wavelet basis is heuristically chosen in the standard WT to capture the most significant features of each defect type. An adaptive wavelet-based feature extractor[25] using a Euclidean distance-based detector was proposed for plain and twill fabric inspection. An undecimated discrete WT was used to extract the fabric features in a multiscale representation and the processed image was partitioned into gray level samples of size $32 \times 32$. This method achieved 97.5% detection accuracy with five known defect types and 93.3% detection accuracy (a slight drop) with three unknown defect types in an evaluation. The method is considered to be reliable because all of the images are of good quality.

The discriminative feature extraction (DFE) method combines the design of the directional wavelet with the design of the detector parameters to minimize the detection error rate. Yang et al.[3] compared six wavelet-based classification methods using various discriminative training approaches on eight defect types of plain and twill fabric. The DFE method using the directional wavelet outperformed the other methods, although the defect classification accuracy slightly decreased to 95.8% in a larger plain fabric database of eight defect types compared to the aforementioned one.[25] From both methods,[3,25] a tailor-made wavelet filter was designed in a shift-invariant representation and based on the characteristics of defects.

In machine learning, a back-propagation NN of a 16-tap Daubechies wavelet decomposition[26] was presented for real-time fabric inspection. The NN used the gray level difference method to characterize the wavelet subimage features. The defect classification accuracy reached 85% (with noise in the input images) and 94% (without noise) for 50 defective and defect-free images. However, to reduce the computational complexity, the device can only implement finite defect types. A three-layer back-propagation NN[4] was suggested for plain white fabric inspection and a defect recognition accuracy of 91.88% was obtained using 160 defective images of four defect types. In this case, the capacity to conduct high-dimensional system modeling using a nonlinear regression algorithm was an advantage. A preprocessed filtering back-propagation network and thresholding of the image analysis were tested on the same kind of fabric in Ref. 27 and 94.38% accuracy was achieved using 240 samples of the four defect classes. Although both methods[4,27] obtained good detection accuracies, the test image quality was poor. The back-propagation NN has the advantage of excellent generalization learning capability due to the ability of learning abstract features of the input (whereas the single-layer network could not), and a tunable inner-layer number with respect to other NNs. However, its shortcomings include a longer training time due to the larger number of inner layers and the danger of over-training.

In summary, besides our previous work on the BB method,[5] few studies have applied the periodicity property of a patterned texture to fabric inspection. In this paper, we extend the previous BB method, which is only controlled by one parameter, by exploiting its directional property for defect detection in plain and twill fabric.

## 3 Directional BB Method

### 3.1 *Formula of BB*

Our previous presentation[5] of the formula of BB for defect detection contained a number of typographical mistakes. An updated definition of the BB is as follows:

**Definition 1.** For a particular row $i$ in an image $X = (x_{ij})$ of size $p \times q$, the middle band (moving average) is defined as

$$\tau_{i,r_m} = \frac{\left(\sum_{j=r_1}^{r_m} x_{ij}\right)}{m}, \tag{1}$$

the upper band is defined as

$$u_{i,r_m} = \tau_{i,r_m} + d \cdot \sigma_{i,r_m}, \tag{2}$$

the lower band is defined as

$$l_{i,r_m} = \tau_{i,r_m} - d \cdot \sigma_{i,r_m}, \tag{3}$$

and $\sigma_{i,r_m}$ is defined as

$$\sigma_{i,r_m} = \sqrt{\sum_{j=r_1}^{r_m} (x_{ij} - \tau_{r_m})^2 / m}, \tag{4}$$

where $d$ denotes the number of standard deviations, denotes the row dimension of the repetitive unit, and $x_{ij}$ is the pixel value at row $i$, column $j$ of the image $X$, the summation of which is from the $r_1$th pixel to the $r_m$th pixel with $1 \le r_1 \le r_m \le q$, $r_m = r_1 + m$, $r_1 \in [1, q-m]$, $r_m = [1+m, q]$, and $\tau_{r_m}, u_{r_m}, l_{r_m} \in R$.

The upper and lower BBs can amplify the defective information after the row and column processing and suppress the information of the patterned texture background. The BB method requires the tuning of two parameters, namely $m$ and $d$, to obtain the optimal detection result. The nominal values for $m$ and $d$ are 20 and 2 (Ref. 28), respectively.

### 3.2 *Mathematical Properties of Directional BB*

**Definition 2.** (Regularity property of a patterned texture) Suppose $m$ and $n$ denote the row and column dimensions of a repetitive unit for any patterned texture image $X = (x_{ij})$ of size $p \times q$. A repetitive unit can generate an entire patterned texture by using a certain translational rule such as a shift in the repetitive unit from $i$ to $i = i + kn$ on a row, or from $j$ to $j + tm$ on a column. The regularity property on a patterned texture image $X = (x_{ij})$ is defined as

$$x_{i+kn,j} = x_{ij} \quad \text{or} \tag{5}$$

$$x_{i,j+tm} = x_{ij} \tag{6}$$

for any integers $k, t \in Z$, $1 \le m$, $1 \le n$, $i + kn \le p$, $j + tm \le q$.

Figure 3 demonstrates the regularity property in the 100th row and 100th column of the plain and twill fabric samples. Regular peaks and valleys can be observed in Fig. 3.

**Lemma 3.** (the shift-invariant property of BB) For the regularity property of any patterned texture image $X = (x_{ij})$, the BB are shift-invariant such that $\tau_{i,r_{m+tm}} = \tau_{i,r_m}$, $u_{i,r_{m+tm}} = u_{i,r_m}$, $l_{i,r_{m+tm}} = l_{i,r_m}$ where $m \times n$ denotes the row and column dimensions of a repetitive unit, and there is a shift of pixel location from $i$ to $i + km$ on a row for any integer $k, t \in Z$.

**Proof.** By the regularity property of the pixels in a patterned texture image $X = (x_{ij})$, a shift-invariant property for middle band BBs on a row can be demonstrated as follows:

$$\tau_{i,r_{m+tm}} = \left(\sum_{j=r_{1+tm}}^{r_{m+tm}} x_{ij}\right)/m = \left(\sum_{j=r_1}^{r_m} x_{i,j+tm}\right)/m = \left(\sum_{j=r_1}^{r_m} x_{ij}\right)/m = \tau_{i,r_m}. \tag{7}$$

Similarly, for the upper and lower bands,

$$u_{i,r_{m+tm}} = \tau_{i,r_{m+tm}} + d \cdot \sigma_{i,r_{m+tm}} = \tau_{i,r_m} + d \cdot \sigma_{i,r_m} = u_{i,r_m}, \tag{8}$$

$$l_{i,r_{m+tm}} = l_{i,r_m}, \text{where} \tag{9}$$

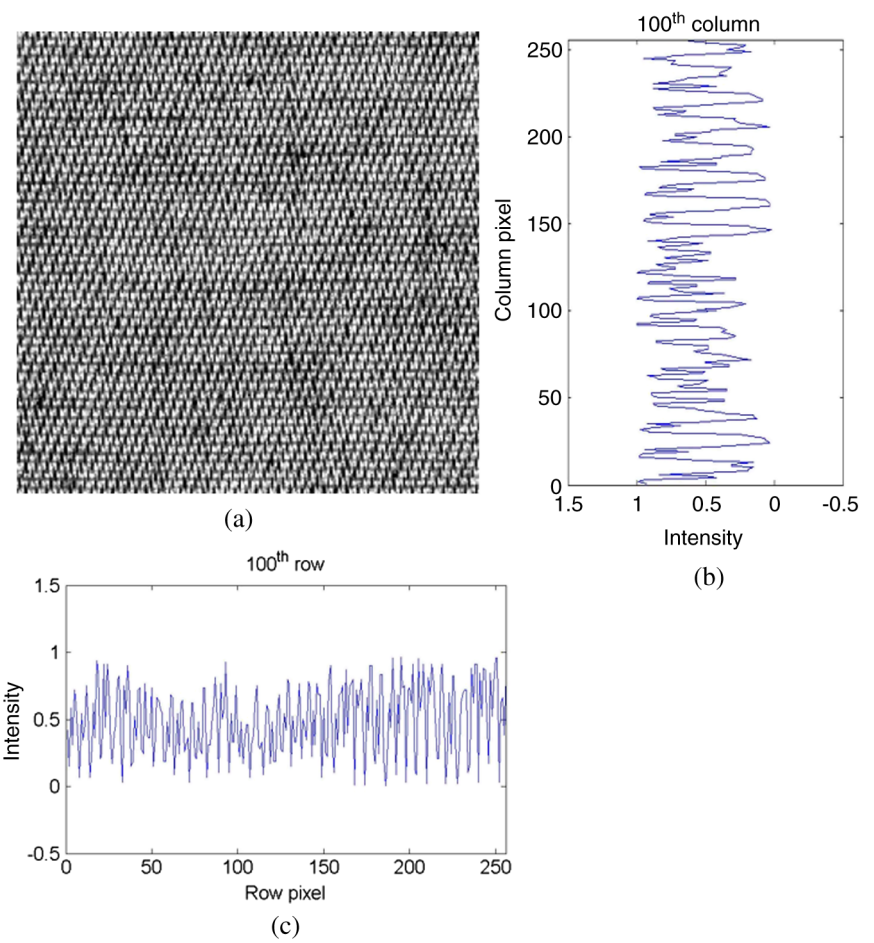


**Fig. 3** (a) Defect-free plain and twill fabric samples of size $256 \times 256$, (b) pixel intensity in the 100th column, and (c) pixel intensity in the 100th row.

$$\sigma_{i,r_{m+tm}} = \sqrt{\sum_{j=r_{1+tm}}^{r_{m+tm}} (x_{ij} - \tau_{j,r_{m+tm}})^2/m}$$
$$= \sqrt{\sum_{j=r_1}^{r_m} (x_{ij} - \tau_{j,r_m})^2/m} = \sigma_{i,r_m}, \quad (10)$$

for any integers $d, t \in Z$, $1 \le m$, $j + tm \le q$. □

Similarly, the same shift-invariant property can be found on the column side for any patterned texture image.

**Remark:** Lemma 3 is also true for the shift-invariant property of BB on the column side.

The shift-invariant property of the BBs allows the upper and lower bands to be sensitive to any change of pixel intensity along a row or a column of a patterned image. Any break in the regularity in a row or a column will be enhanced by the calculation of the BBs, especially by the accentuation of the standard deviation at the upper and lower bands.

**Lemma 4.** (range of BB and the defect detection rules)
For the regularity property of any patterned texture image $X = (x_{ij})$ with a $m \times n$ repetitive unit, the ranges of the upper and lower bands on rows are

$$\tau_{i,r_{m+tm}} + d \cdot \sigma_{i,r_{m+tm}} - e \le u_{i,r_{m+tm}} \le \tau_{i,r_{m+tm}} + d \cdot \sigma_{i,r_{m+tm}} + e \quad (11)$$

and

$$\tau_{i,r_{m+tm}} - d \cdot \sigma_{i,r_{m+tm}} - e \le l_{i,r_{m+tm}} \le \tau_{i,r_{m+tm}} - d \cdot \sigma_{i,r_{m+tm}} + e, \quad (12)$$

where $e$ denotes the error term on the patterned texture image.

Figure 4 shows that the normal range of the upper bands on the rows of a netting multiple defective sample is about [0.5, 1.5]; the errors $e$ are found to be outside this range, which is why the defect detection can only be performed after obtaining the suitable threshold values on the ranges of the upper and lower bands.

**Definition 5.** (Rotation of a patterned image)
For a patterned texture image $X = (x_{ij})$, let $v$ be a basis vector of $X$, such that there exists a nonsingular rotation matrix

$$A = \begin{bmatrix} \cos\theta & \sin\theta \\ -\sin\theta & \cos\vartheta \end{bmatrix}, \quad (13)$$

where $\theta$ represents the degree of rotation from $v$ to $v'$, such that $v' = Av$. In our experiment, two sets of different scales of rotation are applied: $\theta_a = 0$ to 360 deg (over an interval of 30 deg) and $\theta_b = 0$ to 360 deg (over an interval of 45 deg). Due to the symmetry properties of the BB, the rotation angles can be simplified to $\theta = 0$, 30, 45, and 60 deg.

After applying the rotation on a defective image (first row of Fig. 5), four rotated images of degrees $\theta = 0$, 30, 45, and 60 deg are obtained (second row of Fig. 5). The thresholded images of the corresponding rotated images are shown in the third row of Fig. 5. Note that the rotated image has been cropped to the size $180 \times 180$ to maintain the aspect ratio and square shape for processing the directional BB method on the rows and columns. The thresholded image is a binary image where 1 denotes a defective pixel and 0 denotes a defect-free pixel.

After a patterned texture image is rotated, nothing is changed except its geometrical feature (orientation), and hence its regularity property remains. Because the regularity property of the BB is preserved in the rotated images, some defective images with directional defects should be detected at a certain rotation angle. Figure 6 shows an example of a 60-deg rotated image that offers robust detection (the thresholded image in the bottom right of the third row).

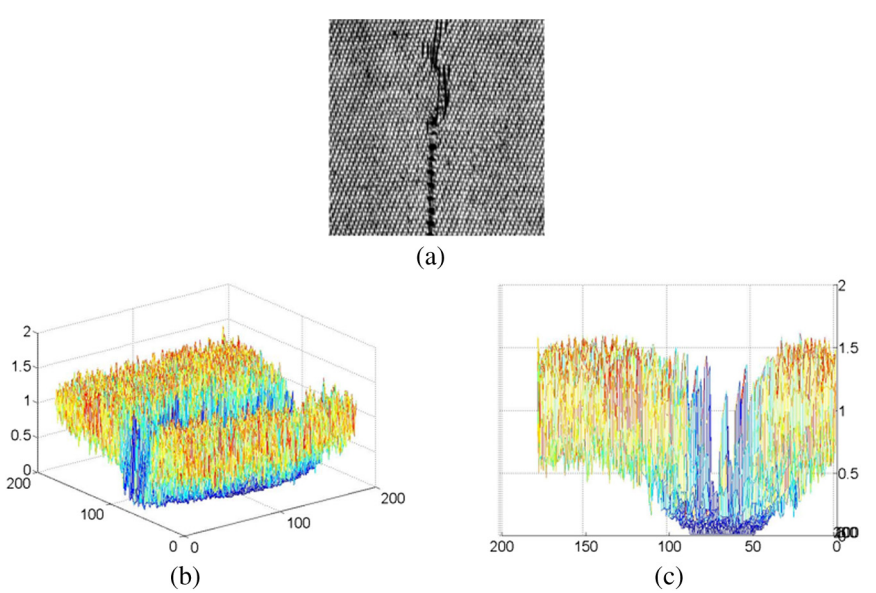


**Fig. 4** (a) Netting multiple sample (n1), (b) side view of upper bands on rows, and (c) longitudinal view of upper bands on rows.

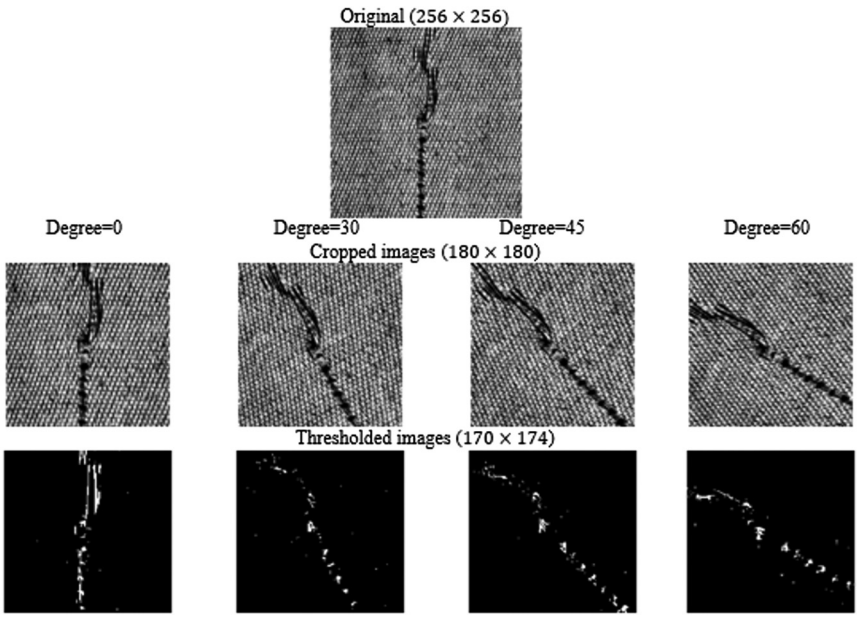


**Fig. 5** (First row) defective sample of netting multiple (n1); (second row) cropped images with rotation angles of 0, 30, 45, and 60 deg; and (third row) thresholded images after the BB processing.

### 3.3 *Procedure of the Directional BB Method*

The procedure of the directional BB approach is given in Fig. 7. The training stage of the directional BB method is as follows:

1. Input the images of the three defect-free plain and twill fabric.
2. Rotate each image around the four orientations of $\theta = 0$, 30, 45, and 60 deg.
3. Apply the BBs on the rows and columns of each rotated image.
4. Obtain the set of threshold values (for details refer to Ref. 5).

The detection stage of the directional BB method comprises the following steps:

1. Input the defect-free or defective test images.
2. Rotate each image around the four orientations of $\theta = 0$, 30, 45, and 60 deg.
3. Apply the BBs on the rows and columns of each rotated image.

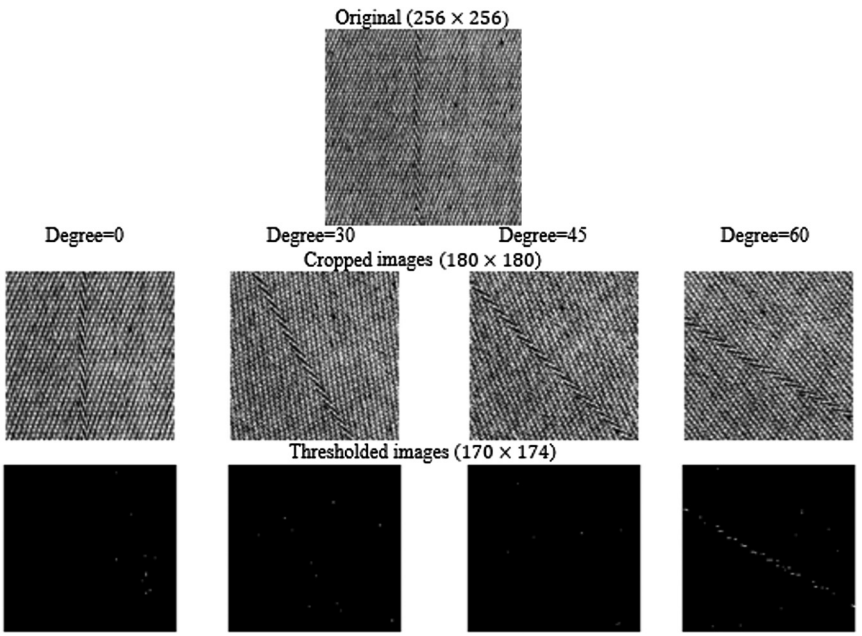


**Fig. 6** (First row) Effectiveness of the directional BB detection approach in a defective wrong draw sample (wd6); (second row) cropped images with rotation angles of 0, 30, 45, and 60 deg; and (third row) thresholded images after the BB processing. The image rotated 60 deg generates a good detection result.

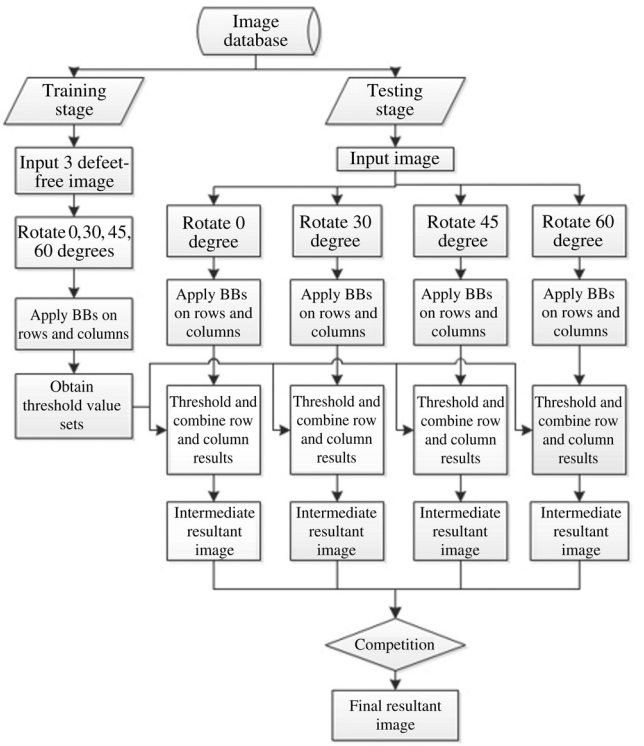


**Fig. 7** Procedure for the directional BB method.

4. Threshold and combine the row and column results.
5. Obtain the intermediate resultant image.
6. The intermediate result with the highest number of white pixels is then selected as the final resultant image.

The intermediate image with the highest number of white pixels is chosen because it is believed that the BBs intersect with the most responsive direction of the defects in the rotated images. It also indicates that rotated image has been tuned to the corrected direction for the directional BB method.

## 4 Performance Evaluation

The evaluation used a database of 100 defect-free and 77 defective images of plain and twill fabric. Each image is of size $256 \times 256$ in 24-bit depth. The performance evaluation involved two phases: (1) determination of the defect detection accuracy by counting the white pixels after thresholding and (2) in-depth evaluation of the detected results using various measurement metrics. The first phase follows the procedure of our previous methods.[5] However, the second phase is newly added to evaluate the degree of success of the proposed method in detecting defects. Herein, a corresponding ground-truth image database for defective images is newly constructed visually in a manually labeled pixel-by-pixel manner for this unpatterned fabric. The ground-truth image is a binary image where 1 indicates a defective pixel and 0 indicates a defect-free pixel. More details of the evaluation are described next. The final resultant defective image of the directional BB method is compared with the ground-truth image to obtain more measurement metrics. Specifically, true positive (TP), true negative (TN), false positive (FP), and false negative (FN) are defined as follows. TP means that the pixels in both the compared image and the ground-truth image are numbered 1, while TN means that the pixels in both the compared image and the ground-truth image are numbered 0. FP means that the pixel of the compared image is 1 but the pixel of the ground-truth image is 0, while FN means the reverse. Based on TP, TN, FP, and FN, several measurement metrics are further defined, as follows: The detection success rate $(\mathrm{DSR}) = (\mathrm{TP}+\mathrm{TN})/(\mathrm{TP}+\mathrm{FP}+\mathrm{TN}+\mathrm{FN})$; the positive predictive value, $(\mathrm{PPV}) = \mathrm{TP}/(\mathrm{TP}+\mathrm{FP})$; and the negative predictive value, $(\mathrm{NPV}) = \mathrm{TN}/(\mathrm{TN}+\mathrm{FN})$. The PPV can be regarded as a precision on the number of TP cases among the number of positive calls in a detection experiment. These metrics help us to determine how the directional BB method performs in analyzing the defective plain and twill fabric samples.

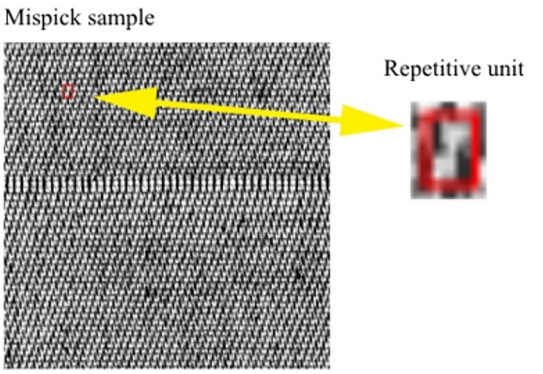


**Fig. 8** A mispick sample and its repetitive unit (highlighted by the red line) of size $7 \times 11$.

In the evaluation, a repetitive unit of an unpatterned fabric is about $7 \times 11$ in size, as shown in Fig. 8. Therefore, the parameters used in the BB method were set to $m = 7$ (the row dimension) and $n = 11$ (the column dimension). As reported in Ref. 5, the final detection result is not greatly affected if the values of $m$ and $n$ are approximately equal to or greater than the lengths of the row and column of a repetitive unit. The standard deviation $\sigma$ is still set to 2 as Ref. 5.

### 4.1 *Intermediate Detection Results for the Four Rotation Angles $\theta = 0$, 30, 45, and 60 deg*

To investigate the robustness of the directional BB method, some intermediate detection results for samples from eight defect types of unpatterned fabric are shown in Fig. 9 (broken end, dirty yarn, mispick, netting multiple, slack end, thick bar B, thin bar, and wrong draw). Herein, all of the images for one defect type have the same orientation. One sample of each defect type is processed by the directional BB method under the four rotation angles: $\theta = 0$, 30, 45, and 60 deg. In Fig. 9, the first row of each defect type illustrates the rotated 0, 30, 45, and 60 deg images, whereas the second row illustrates their corresponding thresholded images before the selection of the final resultant image.

The thresholded image from the 0-deg rotated image can be regarded as the same result as the original BB method.[5] Hence, it is observed that the original BB method can deal with most defect types, especially those with large defects such as dirty yarn [Fig. 9(b)] and defects with a clear appearance, such as the netting multiple [Fig. 9(d)]. However, the

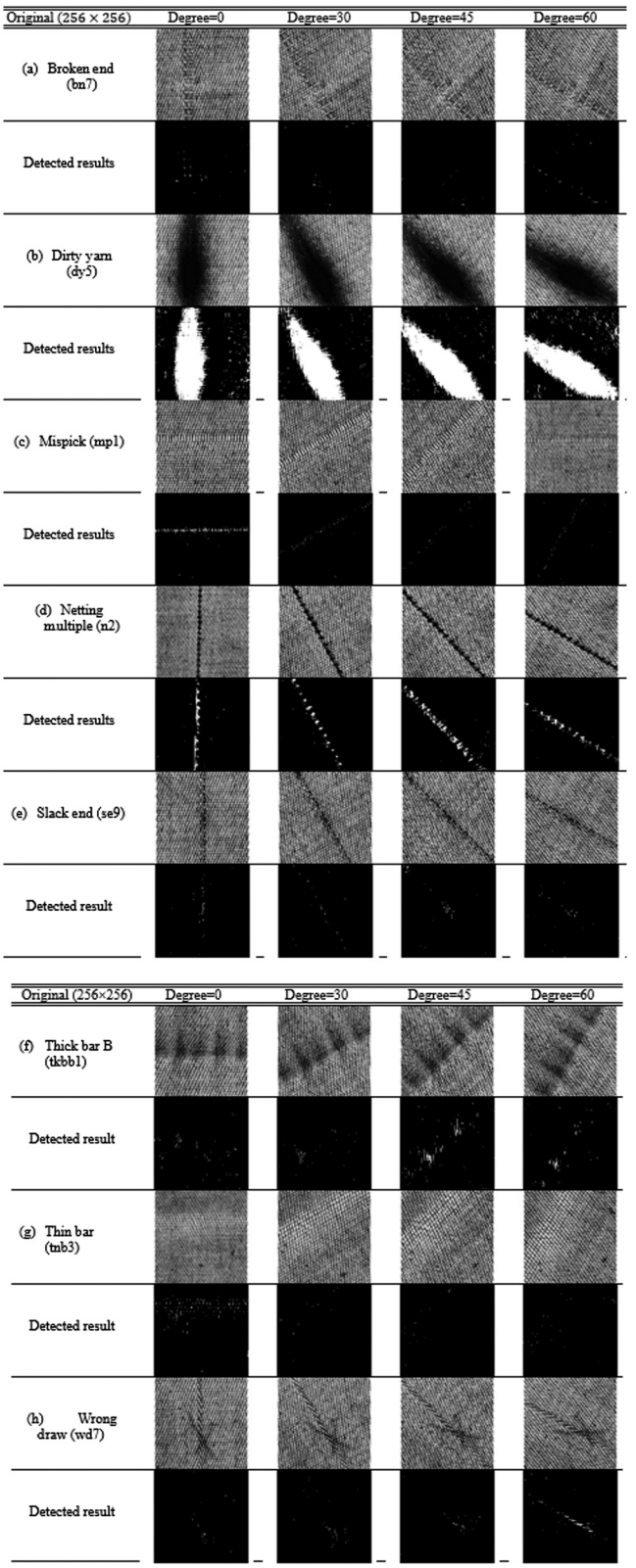


**Fig. 9** (First row of each defect type) cropped defective images ($180 \times 180$) with rotation angles of 0, 30, 45, and 60 deg and their corresponding thresholded images. (Second row of each defect type) thresholded images ($170 \times 174$). (a) Broken end (bn7), (b) dirty yarn (dy5), (c) mispick (mp1), (d) netting multiple, (e) slack end (se9), (f) thick bar B (tkbb1), (g) thin bar (tnb3), and (h) incorrect draw (wd7). The number of samples used is given in parentheses after the defect name.

**Table 1** Average DSR, PPV, and NPV values of the eight types of defective samples.

| | Rot. ang. | DSR | PPV | NPV |
|---|---|---|---|---|
| Broken end (10) | 0 | **98.26** | 3.66 | **98.39** |
| | 30 | 98.11 | 11.19 | 98.18 |
| | 45 | 97.96 | 22.22 | 97.99 |
| | 60 | 98.06 | **31.71** | 98.14 |
| Dirty yarn (7) | 0 | **92.55** | 43.54 | **94.04** |
| | 30 | 91.86 | **46.70** | 92.90 |
| | 45 | 91.06 | 45.43 | 92.96 |
| | 60 | 91.41 | 43.03 | 93.45 |
| Mispick (15) | 0 | **92.68** | 83.92 | **92.79** |
| | 30 | 90.77 | 76.24 | 90.81 |
| | 45 | 90.12 | **88.52** | 90.13 |
| | 60 | 90.96 | 83.27 | 90.97 |
| Netting multiple (7) | 0 | **96.87** | **62.58** | **97.23** |
| | 30 | 95.93 | 60.65 | 96.14 |
| | 45 | 95.45 | 57.75 | 95.74 |
| | 60 | 95.95 | 58.22 | 96.29 |
| Slack end (10) | 0 | **98.38** | 40.29 | **98.47** |
| | 30 | 98.15 | 38.36 | 98.22 |
| | 45 | 97.80 | **41.07** | 97.88 |
| | 60 | 98.11 | 39.84 | 98.19 |
| Thick bar B (10) | 0 | **82.72** | 13.26 | **82.91** |
| | 30 | 80.45 | 40.84 | 80.48 |
| | 45 | 79.31 | **74.74** | 79.33 |
| | 60 | 80.92 | 53.00 | 80.97 |
| Thin bar (10) | 0 | 94.78 | 27.97 | 95.11 |
| | 30 | 95.42 | **43.30** | 95.45 |
| | 45 | **95.89** | 40.50 | **95.92** |
| | 60 | 95.42 | 37.70 | 95.46 |
| Incorrect draw (8) | 0 | **98.21** | 11.90 | **98.26** |
| | 30 | 97.96 | 25.05 | 98.01 |
| | 45 | 97.70 | 36.90 | 97.72 |
| | 60 | 98.12 | **79.23** | 98.17 |

Note: Rot. ang., rotated angle. Bold values represent the largest values and the best performance for that metric.

directional BB method can tackle directional defects with less-clear and relatively smaller appearance such as broken end [Fig. 9(a)], thick bar B [Fig. 9(f)], and wrong draw [Fig. 9(h)]. Table 1 lists the average values of DSR, PPV, and NPV for the 77 defective samples from the eight defect types of unpatterned fabric. The number of samples tested in the evaluation is given in parentheses after each defect type. The DSRs of most of the defect types are more than 90% in any rotated degree, six defect types are over 95%, and three defect types are within 90–95%. Only the thick bar B defect type offers a lower DSR, with the highest being 82.72% for the 0-deg rotated images.

The PPVs (number of positive cases among all positive calls) are consistent with the detection results for the thresholded images of particular rotated images in the directional BB method. If an angle of rotation has a significantly higher PPV than the others, this angle is the most suitable for that defect type in the directional BB method. For example, the thresholded image [Fig. 9(a)] of the 60-deg rotated broken end (bn7) image, the thresholded image [Fig. 9(f)] of the 45-deg rotated thick bar B (tkbb1) image, and the thresholded image [Fig. 9(h)] of the 60-deg rotated incorrect draw (wd7) image generate the best detection results and give much higher PPVs in Table 1. Moreover, the thresholded images of the four rotated images of defects such as dirty yarn (dy5) in Fig. 9(b) and netting multiple (n2) in Fig. 9(d) have very similar PPVs.

**Table 2** Average number of white pixels in the final resultant image for each defect type.

| | Mean | Max | Min | Std |
|---|---|---|---|---|
| Defect-free (100) | 18.79 | 50 | 6 | 9.78 |
| Broken end (10) | 48.20 | 60 | 31 | 8.11 |
| Dirty yarn (7) | 2305.6 | 9260 | 19 | 3277.2 |
| Mispick (15) | 357.47 | 419 | 307 | 34.00 |
| Netting multiple (7) | 407.71 | 778 | 101 | 245.63 |
| Slack end (10) | 55.50 | 77 | 31 | 15.44 |
| Thick bar B (10) | 155.30 | 371 | 56 | 93.32 |
| Thin bar (10) | 149.6 | 255 | 96 | 58.69 |
| Incorrect draw (8) | 75.50 | 149 | 46 | 36.48 |

Note: Std, standard deviation.

**Table 3** Average DSR, PPV, and NPV values of the eight types of defective samples when compared with the ground-truth images.

| | DSR | PPV | NPV |
|---|---|---|---|
| Broken end (10) | 98.20 | 12.70 | 98.34 |
| Dirty yarn (7) | 91.37 | 41.17 | 93.51 |
| Mispick (15) | 92.68 | 83.92 | 92.79 |
| Netting multiple (7) | 96.52 | 55.88 | 96.96 |
| Slack end (10) | 98.12 | 42.69 | 98.22 |
| Thick bar B (10) | 79.94 | 61.85 | 80.00 |
| Thin bar (10) | 94.78 | 27.97 | 95.11 |
| Incorrect draw (8) | 98.12 | 36.90 | 98.17 |
| Overall average | 93.51 | 47.86 | 93.86 |

### 4.2 *Overall Results of the Directional BB Method*

First, regardless of whether an image is defect-free or defective, the average numbers of white pixels in the final resultant images are shown in Table 2. The 100 defect-free images contain an average of 18.79 white pixels whereas the defective images contain from 48.20 (broken end) to 2305.6 (dirty yarn) pixels. In our experiment, a threshold of 40 white pixels is set to determine whether a final resultant image is defective; the defect detection rule is that if the number of white pixels exceeds 40 pixels, the final resultant image is classified as a defective image; otherwise, it is considered defect-free. Four final resultant defect-free images exceed this threshold value and three final resultant defective images (one of broken end and two of slack end) are below the threshold value. Therefore, the error rates for defect-free and defective images are $(4/100) = 4\%$ and $(3/77) = 3.9\%$, respectively. The detection accuracy of simply counting the white pixels on the positive images is 96.05%.

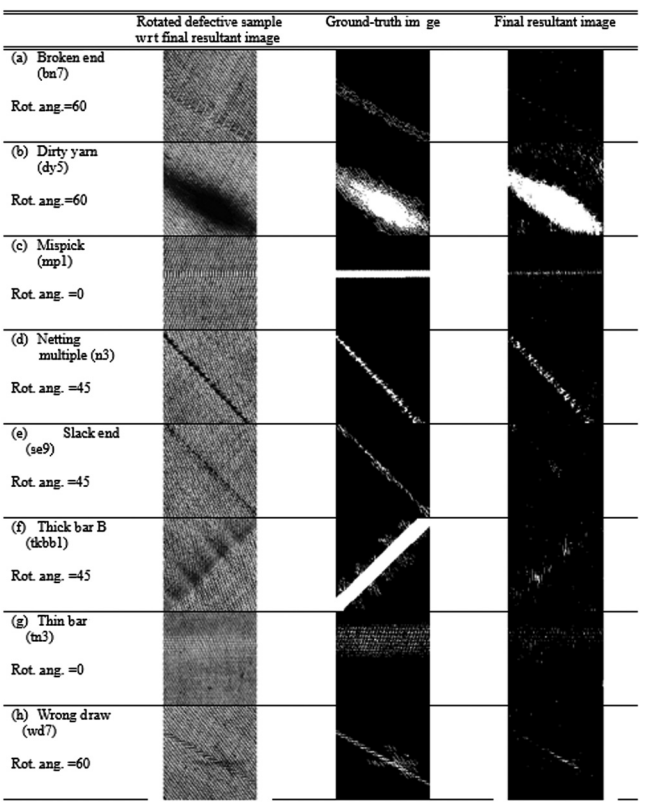


**Fig. 10** Eight types of (second column) rotated defective samples; (third column) the corresponding ground-truth images; and (fourth column) the final resultant images. The selected angles of rotation (rot. ang.) are recorded below each defective sample.

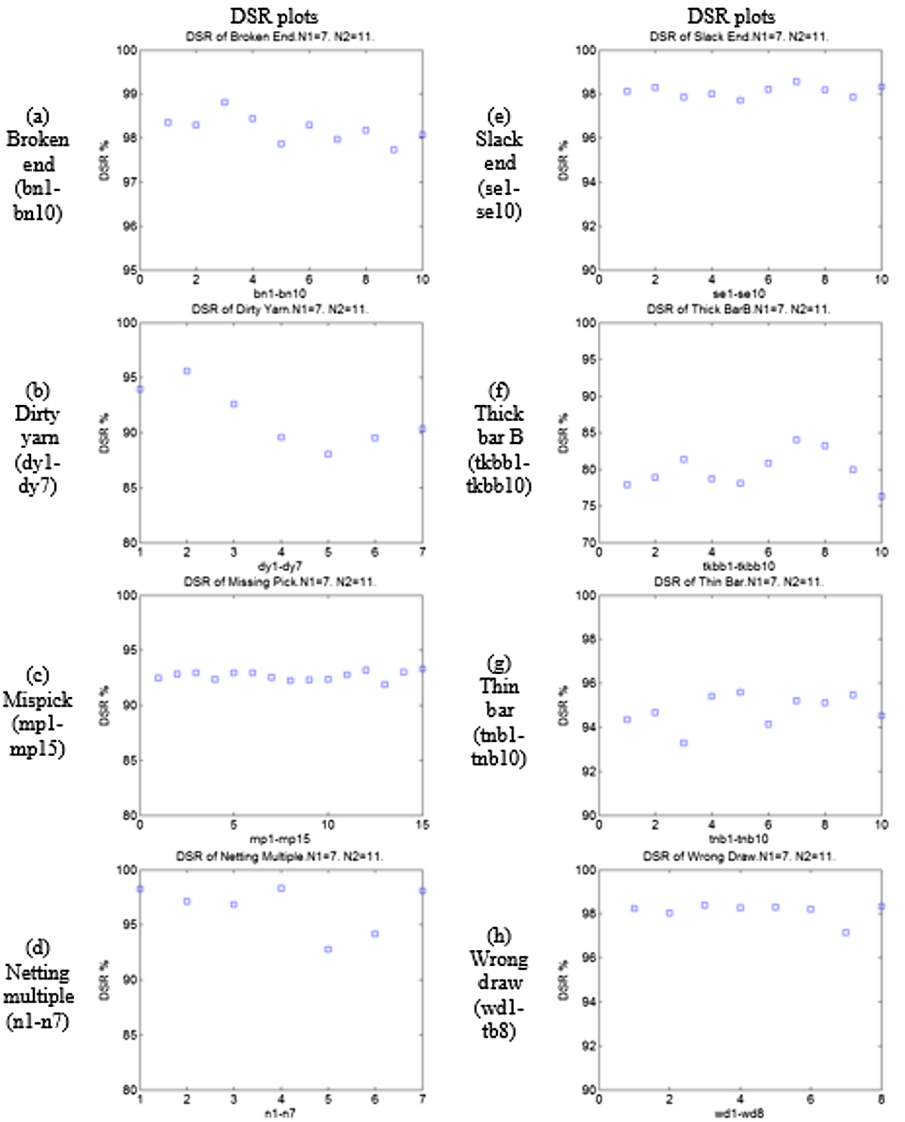


**Fig. 11** The eight defect types and the corresponding DSR plots on the ground-truth images.

We then compare the final resultant images with images from a ground-truth image database in a pixel-by-pixel manner using the various measurement metrics, namely DSR, PPV, and NPV, introduced in Sec. 4.1. Figure 10 illustrates the eight types of rotated defective samples and the corresponding ground-truth and final resultant images. The directional BB method is able to clearly outline the defective regions. Figure 11 shows the corresponding DSR plots on the ground-truth images for each defect type. Table 3 compares the results of the eight defect types and their overall average values: DSR = 93.51%, PPV = 47.86%, and NPV = 93.86%. According to Fig. 11 and Table 3, the

**Table 4** Average values of number of white pixels in each defect type of Canvas-48 in the Outex database in the first phase of the directional Bollinger bands (BB) method in the first phase ($N1 = 5$, $N2 = 5$).

| | Mean | Max | Min | Std |
|---|---|---|---|---|
| Defect-free (20) | 26.60 | 93.00 | 6.00 | 22.43 |
| Dirty yarn (3) | 194.00 | 205.00 | 173.00 | 18.19 |
| Slack end (3) | 69.33 | 86.00 | 50.00 | 18.15 |
| Netting multiple (3) | 291.00 | 346.00 | 255.00 | 41.01 |
| Incorrect draw (3) | 222.00 | 241.00 | 203.00 | 26.87 |

**Table 5** Average DSR, PPV, and NPV values of the four defect-type samples of Canvas-48 in the Outex database when compared with the ground-truth images in the second phase.

| | DSR | PPV | NPV |
|---|---|---|---|
| Dirty yarn (3) | 98.49 | 85.59 | 98.85 |
| Slack end (3) | 97.97 | 69.70 | 98.24 |
| Netting multiple (3) | 97.34 | 46.28 | 99.48 |
| Incorrect draw (3) | 97.17 | 45.23 | 98.95 |
| Overall average | 97.74 | 61.70 | 98.88 |

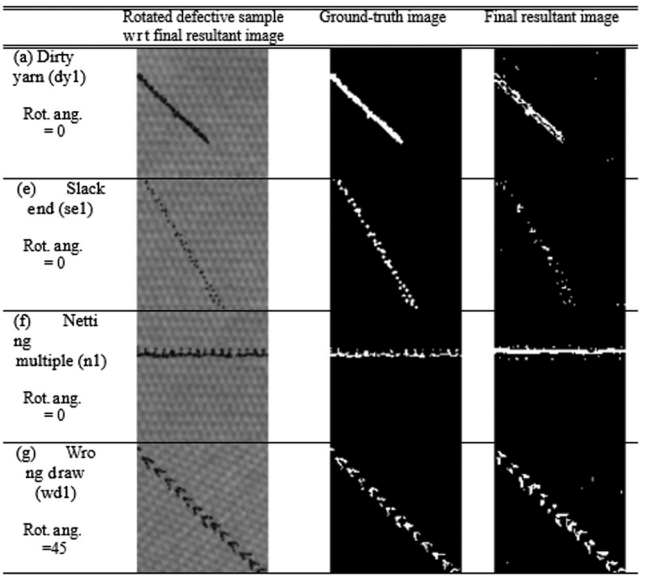


**Fig. 12** Four types of (second column) rotated defective samples; (third column) the corresponding ground-truth images; and (fourth column) the final resultant images. The selected angles of rotation (rot. ang.) are recorded below each defective sample.

broken end, slack end, and wrong draw defects provide the highest DSRs (over 98%), whereas the thick bar B [see Fig. 10(f), for example] defect provides the lowest DSR (around 80%). This result is reasonable because the real defect appearance of the thick bar B [Fig. 10(f) column 2] is scattered and difficult to trace even visually. However, the ground-truth images of thick bar B are labeled as defective in the dilated regions [Fig. 10(f) column 3]. The PPVs are in the range of 12.70% and 83.92%. A high rate is difficult to achieve because the ground-truth images are labeled in a pixel-by-pixel manner and the labeled defect is presented in a discrete format. Therefore, it is very challenging for the detected final resultant image to perfectly match the manually labeled defect.

### 4.3 *Directional BB Method on Outex Database*

In order to verify the reliability of the directional BB method, an extended evaluation has been carried out on the Outex database.[29] As the Outex database contains mostly various natural textures, the samples of the Canvas-48 texture was selected because it is the pattern that is closest in appearance to our research target: unpatterned fabric, in this paper. Since the samples of Canvas-48 texture are all defect-free, four types of defective images: dirty yarn (dy), slack end (se), netting multiple (nn), and wrong draw (wd) are man-made and resembled to the unpatterned fabric database in Sec. 4.2. Each defect type has three samples; hence, a total of 20 defect-free and 12 defective samples from the Outex database for the extended evaluation. Table 4 lists the average number of white pixels in each defect type. The average number of white pixels of defect-free samples after the first phase of the directional BB method is 26.6, which is much lower than four defect-type samples.

**Table 6** Comparison of other methods and directional BB method.

| Method | Wavelet-based[25] | Wavelet-based[3] | GLCM[30] | BB method[5] | Directional BB |
|---|---|---|---|---|---|
| Training | DFE training | Neural network | Unknown | Direct BB calculations | Direct BB calculations |
| Training parameters | Many | Many | Many | The dimensions of the row and column of a repetitive unit | The dimensions of the row and column of a repetitive unit |
| Number of training samples | 240 | 33 | 19 | 3 | 3 |
| Detection level | Partitioned image with a window size of $32 \times 32$. Coarse detection results | Partitioned image with a window size of $32 \times 32$. Coarse detection results | Partitioned image with a window size of $16 \times 16$. Coarse detection results | The whole image. Gives fine detection results | The whole image. Gives fine detection results |
| Fabric | Unpatterned | Unpatterned | Unpatterned | Patterned | Unpatterned |
| Defect types | 8 | 8 | 5 | Less than 8 | 8 |
| Directional defect | Capable | Capable | Unable | Unable | Capable |
| Ground-truth images evaluation | None | None | None | None | Yes |
| Accuracy (based on different setups) | 97.5% on five known defect types; 93.3% on three unknown types | 95.8% | 88.69% | 98.59% | 96.02% detection accuracy; 93.52% DSR on ground-truth images |

**Table 7** Comparison of computational time in the original BB and directional BB methods.

| | Original BB[5] | Directional BB | |
|---|---|---|---|
| | Unpatterned fabric image | Unpatterned fabric image | Outex Canvas-48 image |
| Input image size | $256 \times 256$ | $256 \times 256$ | $128 \times 128$ |
| Rotated and cropped image size | NA | $180 \times 180$ | $90 \times 90$ |
| Processed image size | $256 \times 256$ | $180 \times 180$ | $90 \times 90$ |
| Training time for one image | 11.04 s | 5.61 s | 1.5 s |
| Testing time for one image | 5.16 s | 1.94 s | 3.7 s |

In second phase, the best parameters of $N1$ and $N2$ are 5 in both cases by evaluating the results of dy1 and se1 effective samples, in which the best DSRs are obtained. Table 5 shows the average DSR, PPV, and NPV of all defective samples of the Canvas-48 texture in the Outex database are 97.74%, 61.70%, and 98.88%, respectively. Figure 12 illustrates the best rotated angles for the directional BB method on four-type defective samples of the Canvas-48 texture in the Outex database. It demonstrates the directional BB method offers promising results in this database as well.

### 4.4 *Comparison with Previous Methods for Unpatterned Fabrics*

When the results of the directional BB method are compared with the previous methods, the closest results should be for the wavelet-based defect classification methods[3,25] and the gray-level co-occurrence matrices (GLCM).[30] However, although the wavelet-based methods[3,25] offer good detection results, they require a large number of training samples, significant training time (i.e., NN[3]), and numerous parameters and training samples (e.g., 240 in Ref. 25 and 33 in Ref. 3). Moreover, the wavelet-based detection methods are based on partitioned images with a window of size $32 \times 32$. A GLCM with an NL-means algorithm[30] extracted texture features and achieved 88.69% detection accuracy. Table 6 outlines the differences between the wavelet-based method, the original BB method, and the directional BB method presented in this paper. Table 7 provides a comparison of computational time in the original BB and directional BB methods. The computing facility is a Macbook Air with an Intel i7-4650U CPU and 8 Gb RAM. The directional BB method takes the advantage with a smaller processing size of rotated and cropped image that the computational times in both the training and testing phases are shorter than the original BB method. However, as the borders of the original image are eliminated in the directional BB method, some defect details may be missed. In short, the directional BB method can be seen to offer a fast (compared to the BB method) and efficient defect detection results (compared to previous methods) for unpatterned fabric.

## 5 Conclusion

The directional BB method presented in this paper provides a shift-invariant, fast, and efficient means of detecting defects in unpatterned fabric. Using four rotational representations ($\theta = 0$, 30, 45, and 60 deg). the directional BB method can identify directional defects with less prominent appearance, which was previously untreatable by the original BB method. The average detection accuracy of the directional BB method reaches 96.05% for all defective and defect-free images. Comparison with the ground-truth database of defective images demonstrates a 93.51% DSR on the manually labeled defect locations. Future work can further optimize the algorithm design of the directional BB method to obtain more-clear detected defective regions in the final resultant images. This method can help industrial practitioners to build fast and effective detection methods. This research is beneficial to tile, ceramics, textile, wallpaper, aircraft window, and printed circuit board industries.

### *Acknowledgments*

The first author was supported by Hong Kong Baptist University (HKBU) FRG Grant 12-13/075.

### *References*

1. H. Y. T. Ngan, G. K. H. Pang, and N. H. C. Yung, "Automated fabric defect detection—a review," *Image Vision Comp.* **29**(7), 442–458 (2011).
2. H. Y. T. Ngan, G. K. H. Pang, and N. H. C. Yung, "Motif-based defect detection for patterned fabric," *Pattern Recognit.* **41**(6), 1878–1894 (2008).
3. X. Z. Yang, G. K. H. Pang, and N. H. C. Yung, "Discriminative training approaches to fabric defect classification based on wavelet transform," *Pattern Recognit.* **37**(5), 889–899 (2004).
4. C.-F. J. Kuo, C. Lee, and C. Tsai, "Using a neural network to identify fabric defects in dynamic cloth inspection," *Text. Res. J.* **73**(3), 238–244 (2003).
5. H. Y. T. Ngan and G. K. H. Pang, "Novel method for patterned fabric inspection using Bollinger bands," *Opt. Eng.* **45**(8), 087202 (2006).
6. H. Y. T. Ngan et al., "Wavelet based methods on patterned fabric defect detection," *Pattern Recognit.* **38**(4), 559–576 (2005).
7. H. Y. T. Ngan and G. K. H. Pang, "Regularity analysis for patterned texture inspection," *IEEE Trans. Autom. Sci. Eng.* **6**(1), 131–144 (2009).
8. C. J. Kuo and T. Su, "Gray relational analysis for recognizing fabric defects," *Text. Res. J.* **73**(5), 461–465 (2003).
9. F. Tajeripour, E. Kabir, and A. Sheikhi, "Fabric defect detection using modified local binary patterns," *EURASIP J. Adv. Sig. Process.* **2008**, 783898 (2008).
10. H. Y. T. Ngan, G. K. H. Pang, and N. H. C. Yung, "Performance evaluation for motif-based patterned texture defect detection," *IEEE Trans. Autom. Sci. Eng.* **7**(1), 58–72 (2010).
11. D. Tsai and T. Huang, "Automated surface inspection for statistical textures," *Image Vision Comp.* **21**, 307–323 (2003).
12. E. J. Wood, "Applying Fourier and associated transforms to pattern characterization in textiles," *Text. Res. J.* **60**, 212–220 (1990).
13. C. Casterllini et al., "On-line textile quality control using optical Fourier transforms," *Opt. Lasers Eng.* **24**, 19–32 (1996).
14. L. M. Hoffer et al., "Neural network for the optical recognition of defects in cloth," *Opt. Eng.* **35**(11), 3183–3190 (1996).
15. S. H. Chiu, S. Chou, and J. J. Liaw, "Textural defect segmentation using a Fourier-domain maximum likelihood estimation method," *Text. Res. J.* **72**(3), 253–258 (2002).

16. C. H. Chan and G. K. H. Pang, "Fabric defect detection by Fourier analysis," *IEEE Trans. Ind. Appl.* **36**(5), 1267–1276 (2000).
17. A. Kumar and G. K. H. Pang, "Defect detection in textured materials using Gabor filters," *IEEE Trans. Ind. Appl.* **38**(2), 425–440 (2002).
18. A. K. Jain and F. Farrokhnia, "Unsupervised texture segmentation using Gabor filters," *Pattern Recognit.* **24**(12), 1167–1186 (1991).
19. J. Escofet et al., "Detection of local defects in textile webs using Gabor filters," *Opt. Eng.* **37**(8), 2297–2307 (1998).
20. D. M. Tsai and S. K. Wu, "Automated surface inspection using Gabor filters," *Int. J. Adv. Manuf. Technol.* **16**, 474–482 (2000).
21. L. Ding et al., "Gabor filter based automatic textile defect detection," *Proc. SPIE* **4875**, 789–795 (2002).
22. A. Bodnarova, M. Bennamoun, and S. Latham, "Optimal Gabor filter for textile flaw detection," *Pattern Recognit.* **35**, 2973–2991 (2002).
23. H. Sari-Sarraf and J. S. Goddard, "Vision system for on-loom fabric inspection," *IEEE Trans. Ind. Appl.* **35**(6), 1252–1259 (1999).
24. H. S. Sarraf and J. S. Goddard Jr., "Robust defect segmentation in woven fabrics," in *Proc. IEEE Conf. Computer Vision and Pattern Recognition (CVPR1998)*, pp. 938–944 (1998).
25. X. Z. Yang, G. K. H. Pang, and N. H. C. Yung, "Discriminative fabric defect detection using directional wavelets," *Opt. Eng.* **41**(12), 3116–3126 (2002).
26. Y. A. Karayiannis et al., "Defect detection and classification on web textile fabric using multiresolution decomposition and neural networks," in *Proc. 6th IEEE Int. Conf. Electronic, Circuits & Systems (ICECS1999)*, Vol. 2, pp. 765–768 (1999).
27. C.-F. J. Kuo and C. Lee, "A back-propagation neural network for recognizing fabric defects," *Text. Res. J.* **73**(2), 147–151 (2003).
28. J. Bollinger, *Bollinger on Bollinger Bands*, McGraw-Hill, New York (2001).
29. University of Oulu, "Extended Outex texture classification test suites," http://lagis-vi.univ-lille1.fr/datasets/outex.html (27June2015).
30. H. Zuo et al., "Fabric defect detection based on texture enhancement," in *IEEE 5th Int. Congress on Image and Signal Processing*, pp. 876–880 (2012).

**Henry Y. T. Ngan** received his BSc (Math), MPhil, and PhD (EEE) degrees from University of Hong Kong, China, in 2001, 2005, and 2008, respectively. He is a research assistant professor in the Department of Mathematics, Hong Kong Baptist University. He has published over 30 publications. His current research is inspection and metrology applications on anomaly detection, large-scale data analysis, social signal processing, visual surveillance, transportation, and medical imaging. He is a senior member of the IEEE.

**Grantham K. H. Pang** received his PhD degree from University of Cambridge in 1986. Currently, he is an associate professor in the Department of Electrical and Electronic Engineering, University of Hong Kong, China. He has published over 160 technical papers, authored/coauthored six books, and obtained five U.S. patents. His research interests include machine vision for surface defect detection, video surveillance, expert systems for control system design, intelligent control, and intelligent transportation systems.